J. Water Environ. Nanotechnol., 8(2): 190-205 Spring 2023

ORIGINAL RESEARCH PAPER

Influence of CTAB surfactant on the various properties of CdO nanoparticles and their application in field of dye degradation

Deepak Singhwal[1], Amita Khatri[1] and Pawan S. Rana[1*]

[1]Department of Physics, Deenbandhu Chhotu Ram University of Science & Technology, Murthal, Sonipat 131039, Haryana, India

Received: 2022-09-17 Accepted: 2022-12-04 Published: 2023-05-23

ABSTRACT

By co-precipitation, cetyltrimethylammonium bromide (CTAB) assisted CdO nanoparticles with different CTAB concentrations (0.0M, 0.04M, 0.08M, and 0.12M) have been synthesized and evaluated for potential photocatalytic applications. X-Ray Diffraction (XRD) results indicate that crystallite size increases as the concentration of CTAB is increased. Field Emission Scanning Electron Microscope (FESEM) exhibits that flat sheet-like morphology is changing into a thin needle-like structure with a concentration of surfactant. Elemental Dispersive X-ray Spectroscopy (EDS) confirmed the existence of constituents and hence marks the purity of prepared samples. The broad peak of Raman spectra is consisting of three bands from 200-500 cm^{-1} while Fourier Transform Infrared (FTIR) spectra certify vibration of Cd and O bonds are present at 530 cm^{-1}. The optical band gap is found to slightly decrease due to the addition of CTAB. The results of the experiment showed that CdO nanoparticles degraded Methylene Blue (MB) up to 83% in UV light, and Rose Bengal (RB) dye up to 85% in sunlight within 80 minutes of exposure.

Keywords: Coprecipitation, CTAB, Methylene Blue, and Photocatalysis.

How to cite this article

Singhwal D., Khatri A., Rana P. S., Influence of CTAB surfactant on the various properties of CdO nanoparticles and their application in field of dye degradation. J. Water Environ. Nanotechnol., 2023; 8(2): 190-205 DOI: 10.22090/jwent.2023.02.008

INTRODUCTION

Humans are now very concerned about the threat posed by water pollution. A solution to this issue is being sought by researchers. Our drinking water resources are becoming contaminated as a result of the increased industrialization and the numerous sorts of untreated industrial pollutants that are being produced. Water pollution is now largely caused by dyes that come from many businesses, including the leather, textile, and pharmaceutical sectors [1]-[5]. These colors are extremely dangerous for aquatic life as well as humans and are carcinogenic. For the management of dye wastewater, a variety of techniques including ion exchange, adsorption, filtration, and coagulation have been used. One of these techniques, the photocatalytic process, is useful in advanced oxidation processes[6]-[8]. In this process, mainly electrons and holes take part to carry the reaction **[9]–[11]** as shown in Fig.1.

Due to their physical and chemical differences from bulk materials, nanomaterials, particularly oxides, are shown to be effective photocatalysts for the degradation of dyes [12]. They also have a bigger surface area due to their smaller size, which results in more electrons and holes coming to the surface to participate in chemical reactions. This leads to the maximum efficiency in dye degradation in the shortest amount of time. The first substance employed as a photocatalyst was TiO_2 nanomaterial, and afterward, numerous compounds have been researched [13]. There are a variety of factors in the photocatalytic process that we can manage to develop the desired material for our purposes. CdO nanoparticles

* Corresponding Authors Email: *drpawansrana.phy@dcrustm.org*

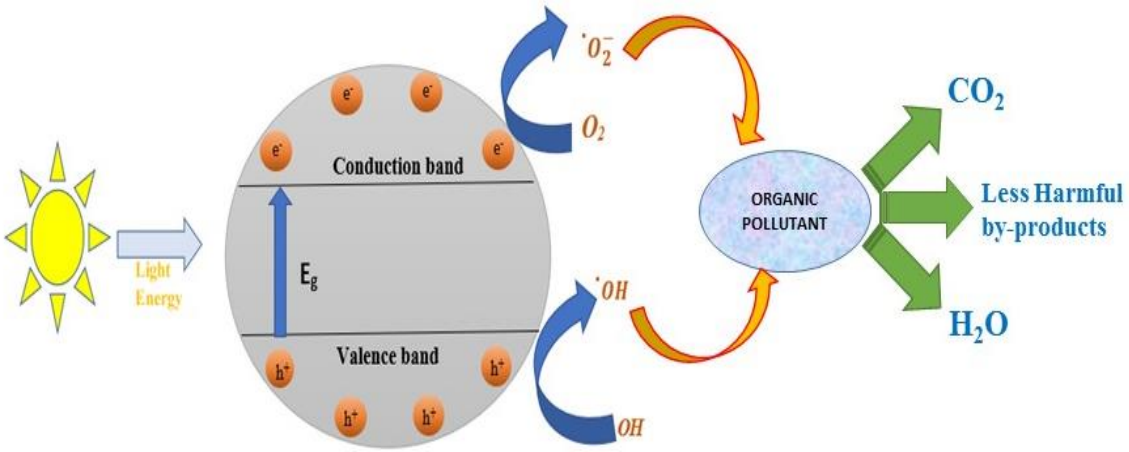

Fig. 1. Production of superoxide and hydroxyl radicals from electrons and holes.

have become increasingly important in recent years for photocatalytic applications. With an optical band gap energy of between 2.2 and 2.7 eV, the N-type nature of the CdO semiconductor makes it appropriate for photocatalytic use [14]-[22]. Because of its narrow optical band gap, CdO functions well as a photocatalyst for dye degradation in UV and visible light. CdO has numerous uses in optoelectronics devices in addition to being a photocatalyst. It is a leading oxide among transparent conducting oxides [23]-[27]. CdO is a material that works well in solar and photovoltaic cells because of its high electrical conductivity and increased carrier mobility [28]-[33]. Nanoparticles can be created using a variety of techniques, including hydrothermal, co-precipitation, and sol-gel. But in this study, cadmium oxide nanoparticles are prepared using a co-precipitation process. By regulating the pH and temperature of the process, this approach offers an easy way to create nanoparticles [34]-[38]. Compared to other methods, it takes less time and has a good yield. As we all know, the narrow band gap in CdO causes the quick recombination of electrons and holes created by light source irradiation. The effectiveness of CdO in photocatalytic processes is not particularly great because abrupt recombination prevents electrons and holes from participating in chemical reactions. Large-scale research has been conducted in the last several years to determine the effects of surfactant addition on the various characteristics of nanomaterials. But as of right present, it's unclear which factors govern how nanoparticles develop when surfactants are added. There is still more to learn about the different aspects that influence how nanoparticles grow. Whether the surfactant is cationic, anionic, or neutral, its nature also matters. Hence, the role of CTAB concentrations on the extensive properties of CdO nanoparticles has been discussed in this supporting work, as well as how CTAB concentrations affect the photocatalytic activity of CdO nanoparticles. It is important to recognize that surfactants play a major role in the synthesis of nanoparticles. By using surfactants, particles can be prevented from aggregating. There is a decrease in the surface energy of a solution when surfactants are present [39]. CTAB is a cationic surfactant that means positively charged head and is hydrophilic as shown in Fig. 2 **[40]**.

Cationic surfactants are only 5-6% of the production of all types of surfactants still they have their importance. The positive charge of the cationic surfactant makes them effective because they get easily adsorb on the negative charge in solid even at neutral pH. In the present work, a series of CTAB-assisted CdO nanoparticles have been synthesized using the coprecipitation method followed by the characterization of synthesized samples using X-Ray Diffraction (XRD), Field Emission Scanning Electron Microscopy- Energy Dispersive X-Ray Spectroscopy (FESEM-EDS), Raman Spectroscopy, Fourier Transform Infrared Spectroscopy (FTIR) and Diffused Reflectance Spectroscopy (DRS). As model pollutants, Methylene Blue (MB) dye and Rose Bengal (RB) dye have been used to investigate the effect of surfactant addition on the photocatalytic properties of CdO.

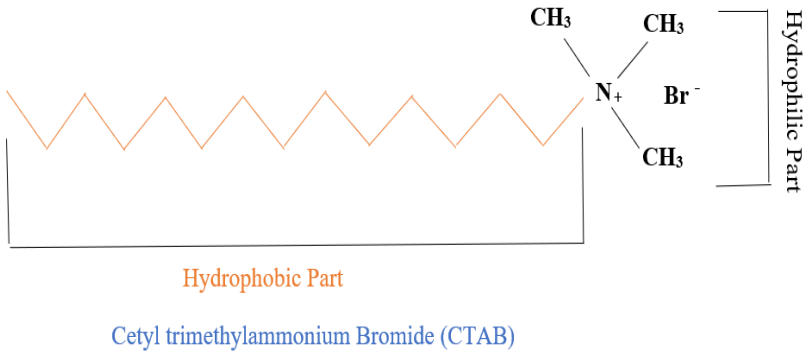

Fig. 2. Structure of CTAB surfactant.

EXPERIMENTAL METHOD

Materials

Most of the chemicals used in our research were bought from loba chemie and used directly after purchase without further purification. Cadmium nitrate tetrahydrate [$Cd(NO_3)_2.4H_2O$] of 99% purity was purchased from Merck. From Fisher Scientific, MB dye was bought. Water that had been twice distilled was used for the entire synthesis. Reagents like sodium hydroxide (NaOH) flakes with 98% and cetyltrimethylammonium bromide ($C_{19}H_{42}BrN$) with 99% are classified as an annular grade.

Formation of nanoparticles

Cadmium nitrate tetrahydrate [$Cd(NO_3)_2.4H_2O$] with 99% purity in distilled water is used in the co-precipitation process to produce pure CdO nanoparticles. To increase the pH of the cadmium salt solution, 100 ml of freshly made 1M solution of NaOH was added drop by drop for a half-hour while the solution was continuously stirred at 40 °C. Then after one hour of the constant stirring solution was placed undisturbed to settle the precipitates. Filters were then used to remove precipitates, which were subsequently washed with distilled water several times. An annealing procedure of four hours at 400 ^{0}C was used for washed samples. The sample so prepared was named CC0.

$Cd(NO_3)_2.4H_2O + 2NaOH \rightarrow Cd(OH)_2 + 4H_2O + 2NaNO_3$ **(Step 1)**

$Cd(OH)_2 \rightarrow CdO + H_2O$ After heating **(Step 2)**

Similarly, for the synthesis of CTAB-assisted CdO nanoparticles with various concentrations of CTAB, the same method is adopted. 0.04M, 0.08M, and 0.12M solution of surfactant was prepared separately. Before the addition of the base, the solution of surfactant and the solution of precursor were mixed properly with continuous stirring for 30 minutes. CTAB-assisted CdO nanoparticles with different concentrations of CTAB 0.0M, 0.04M, 0.08M, and 0.12M are named CC0, CC4, CC8, and CC12 respectively.

Characterization of the materials.

XRD (X-Ray Diffraction)

To determine whether the structure of the samples is crystalline or amorphous, X-ray diffraction (XRD) was carried out using a Rigaku Ultima IV diffractometer (λ = 1.54 Å of Cu-k_α radiation) at room temperature with a copper anti-cathode operated at 40 kV and 40 mA. To perform diffraction, powder samples were evenly spread out on a neutral quartz glass sample holder, exposed to a k-alpha radiation source, and scanned between 10° and 80° angles.

FESEM with EDS

The sample's size, shape, and surface morphology were examined under a nova-nano FESEM 450 (FEI) microscope. For a high-resolution image in this equipment, highly accelerated electrons are used instead of a light beam. Secondary electrons are released and collected by the detector as a result of the striking of electrons on the material surface, aiding in the analysis of the material's composition.

BET analysis

One of the most crucial measurements for describing innovative porous materials is the surface area. The most common technique for calculating surface areas from nitrogen adsorption isotherms is the BET analysis.

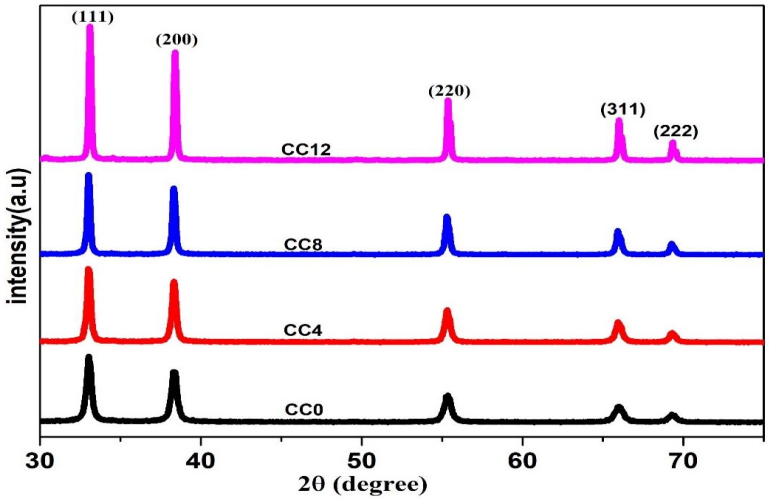

Fig. 3. XRD pattern for CC0, CC4, CC8 and CC12.

Raman Spectroscopy

Raman spectroscopy is a spectroscopic method for identifying rotational, vibrational, and other states in a molecular system that can be used to examine the chemical components of materials. STR 500 Confocal Micro Raman spectrometer having DPSS laser source is used for Raman spectra.

Fourier Transform Infrared Spectroscopy (FTIR)

An analytical method called FTIR is used by material analysts to determine the chemical constitution of a sample. FTIR spectra of the KBr pallets with sample and KBr powder ratio of 5:95 was recorded with the help of FT-IR Spectrum 2 Perkin Elmer instrument in wavenumber range 4000cm^{-1} to 400 cm^{-1}.

Diffused Reflectance Spectroscopy

To gather molecular spectroscopic data, diffuse reflectance, an optical phenomenon, is frequently used in the UV-visible, near-infrared (NIR), and mid-infrared wavelength ranges. The band gap of the semiconducting material can be calculated using this technique. Range of 200 nm to 1200 nm of Spectrophotometer LAMBDA 750 Perkin Elmer UV-Vis NIR is used for diffused reflectance spectra.

Photocatalytic reaction

By applying a 300W UV lamp to process MB dye on the samples, the photocatalytic performance of the samples was examined. First, a lab-made 5ppm (5mg/L) MB dye solution was prepared. The 50 ml of MB dye solution was combined with 50 mg of CC0 nanoparticles. The solution was mixed for several minutes in the dark to ensure absorption-desorption equilibrium before exposing to UV light. Aliquots of 5 ml from the solution were taken every 20 minutes after the UV lamp was turned on. The same process was carried out again for CC4, CC8, and CC12. The photocatalytic performance of the sample is evaluated from absorption spectra recorded by the LABINDIA UV 3092 UV-VIS Spectrophotometer. Degradation (%) is calculated from the formula:

$$\textbf{Degradation (\%)} = \frac{(A_0 - A_t)}{(A_0)} \textbf{ x 100} \qquad \textbf{(1)}$$

Here, A_0 represents the absorbance intensity of dye before keeping it in UV light, and A_t symbolizes the absorbance intensity of dye at any instant '*t*' after irradiation of the sample [**41**]. The same procedure has been repeated for RB dye but in the presence of visible light.

OUTCOMES AND DISCUSSION

X-Ray Diffraction Analysis

Fig. 3. is showing X-Ray Diffraction pattern of prepared samples. Formation of CC0, CC4, CC8, and CC12 is confirmed by X-Ray Diffraction peaks (111), (200), (220), (311), and (222) which are appearing at angles 33.04°, 38.34°, 55.32°, 65.94° and 69.30° respectively. According to JCPDS card no 05-0640, this diffraction pattern of CdO confirms the formation of cubic structure [**42**]. Calculation of Crystallite size *(D)* is done with the help of Debye-Scherrer's equation:

$$D = \frac{k\lambda}{\beta\, Cos(\theta)} \qquad \textbf{(2)}$$

Here, D represents crystallite size, k = 0.94 is

Table 1. Parameters (D, a, and E_g) were calculated from the XRD and DRS spectra of the prepared samples.

Sample	Crystallite Size, D (nm)	Lattice parameter, a (Å)	Microstrain, ε (x 10^{-3})	Optical band gap E_g (eV)
CC0	23.89	4.69	1.45	2.29
CC4	30.13	4.69	1.15	2.24
CC8	40.76	4.69	0.85	2.26
CC12	47.79	4.69	0.72	2.24

a constant, λ is the wavelength of X-ray which is 1.54 Å, β stands for full width at half maximum (FWHM) and θ is half of the angle at which peak is located [**43**]. Crystallite sizes for CC0, CC4, CC8, and CC12 are found to be 23.89 nm, 30.13 nm, 40.76 nm, and 47.79 nm respectively. As the surfactant concentration rises, the crystallite's size expands. As surfactant concentration rises, the amount of thermal energy available for recrystallization decreases, lowering full-width half maxima [**44**]. The term "critical micelle concentration" (CMC) refers to the level of surfactant in a bulk phase above which micelles, which are aggregates of surfactant molecules, start to form. Surfactants have an important characteristic called the CMC. The CMC of CTAB is 0.0009 mol/L in water. Working at concentrations over CMC may result in micelles binding to the surface of the nanoparticles. This may cause hydrophobic interactions between nanoparticles and agglomeration to take place. By increasing the surfactant concentration, produced samples exhibit increased crystallinity and decreased microstrain due to hydrophobic interaction between the surfactant molecules rather than host lattice substitution. Because the peaks are not shifting, the lattice parameter is also the same. Diverse parameters calculated from favored orientation (111) are tabulated in Table 1. Microstrain (ε) is calculated using the equation:

$$\varepsilon = \frac{\beta \cos(\theta)}{4} \quad (3)$$

The lattice parameter is evaluated from the equation:

$$d^2 = \frac{a^2}{(h^2+k^2+l^2)} \quad (4)$$

here d denotes interplanar spacing, a denotes lattice parameter and *(hkl)* represents the miller indices.

FESEM-EDS Analysis

FESEM has been used to examine the morphology of prepared materials. The FESEM images of CC0, CC4, CC8, and CC12 are shown in Fig. 4(a-d). In Fig. 4(a), the nanosheet-like structure of CdO is visible, and these nanosheets are also forming an arrangement that resembles a flower. However, if the surfactant concentration is increased, these sheets-like structures begin to fragment into smaller pieces (in the shape of a needle), as shown in Fig. 4 (b). Due to further enhancement in the amount of CTAB, agglomeration of particles and growth of needles on the surface of the agglomerated particles takes place, as shown in Fig. 4(c). At 0.12M concentration of CTAB, a clear picture of stronger agglomeration along with dense growth of needles can be seen in Fig. 4(d). Based on the described results, it is observed that increasing the mass of the surfactants affects nanoparticle formation. The formation of these morphologies is caused by the self-assembly of surfactant molecules within micelles. Only when the concentration of the surfactant molecules surpasses the critical micelle concentration (CMC) do they begin to self-assemble into micelles, which lowers the solvent/surfactant interface and minimizes interactions between the hydrophobic and hydrophilic components. This dual nature causes them to be both attracted to and repellent to the solvent, resulting in the self-assembly process. FESEM images conclude that the addition of surfactant aligns the nanoparticles in a particular direction by forming needles. Energy Dispersive X-Ray spectra are also obtained for the detection of elemental composition as shown in Fig. 5(a-d). From EDS, it is confirmed that Cd and O elements are present in good proportion. The presence of carbon element is also shown by spectra which is due to the carbon grid on which the sample was mounted for FESEM.

BET analysis

Surfactants cause changes to surface area in addition to morphology. Therefore, we used BET to analyze our sample and found that the surface area (Table 2) had grown from 6.687 m^2/g to 37.301 m^2/g. Pore volume is also enhanced. The pores' diameter decreases. The specific surface area and

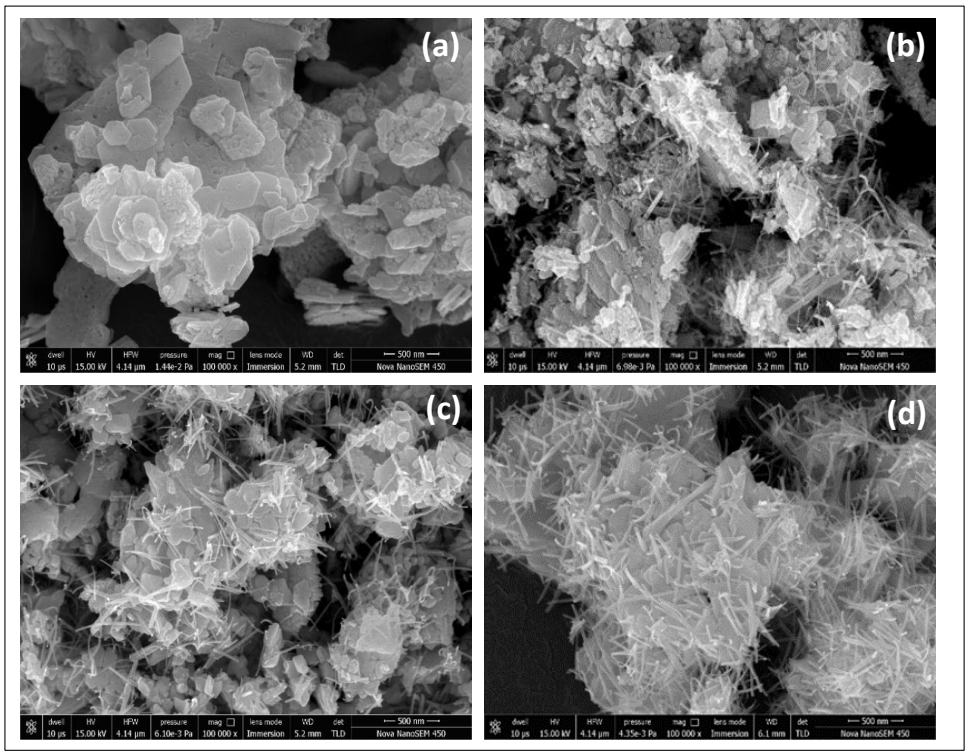

Fig. 4. For structural analyses, FESEM images of (a) CC0 (b) CC4 (c) CC8 (d) CC12.

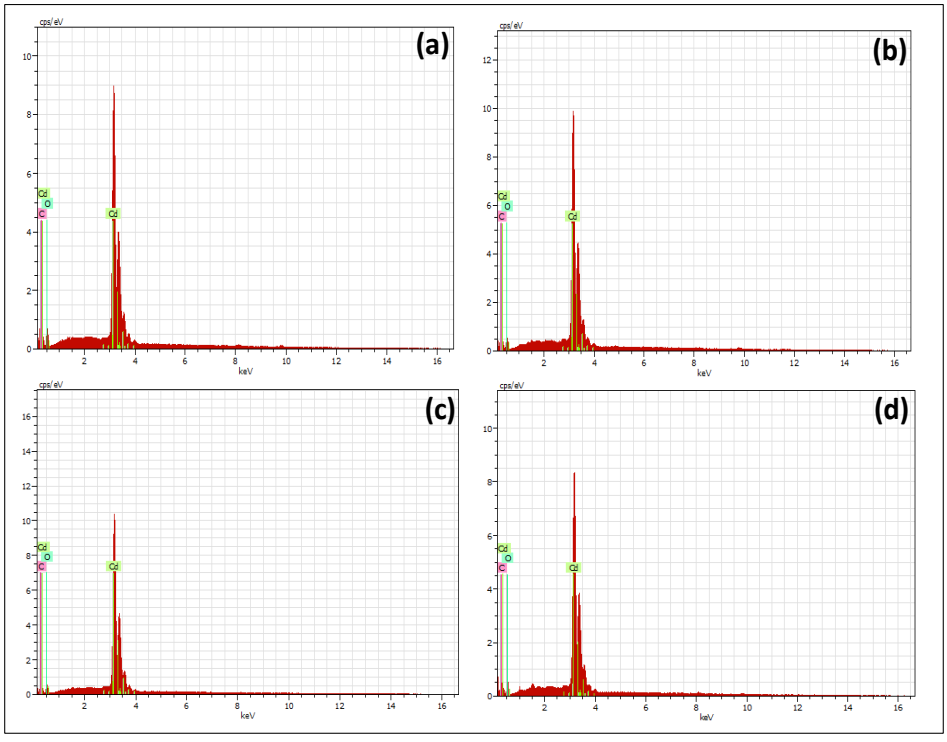

Fig. 5. For quantitative analyses of chemical composition, EDS images of (a) CC0 (b) CC4 (c) CC8 (d) CC12.

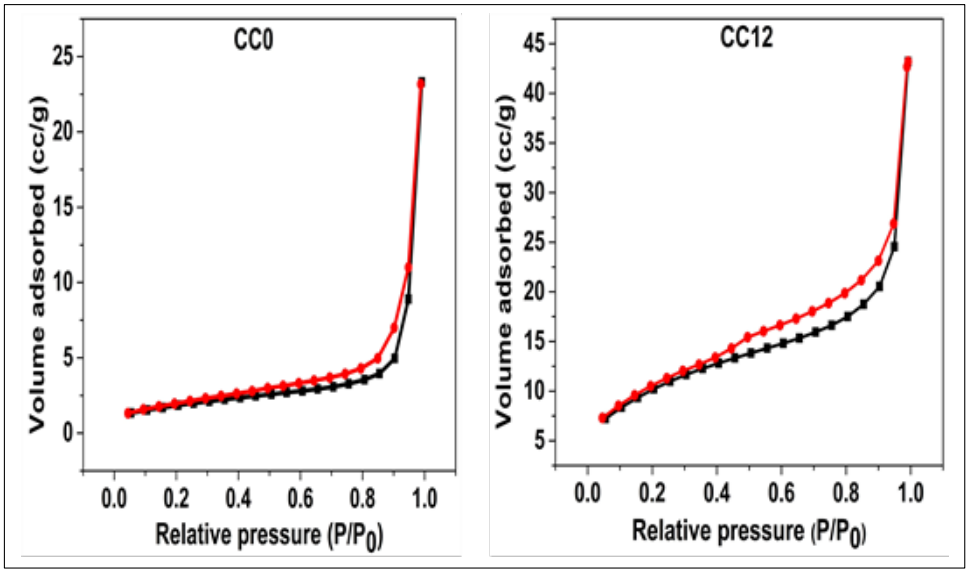

Fig. 6. Nitrogen adsorption-desorption isotherms of CC0 and CC12.

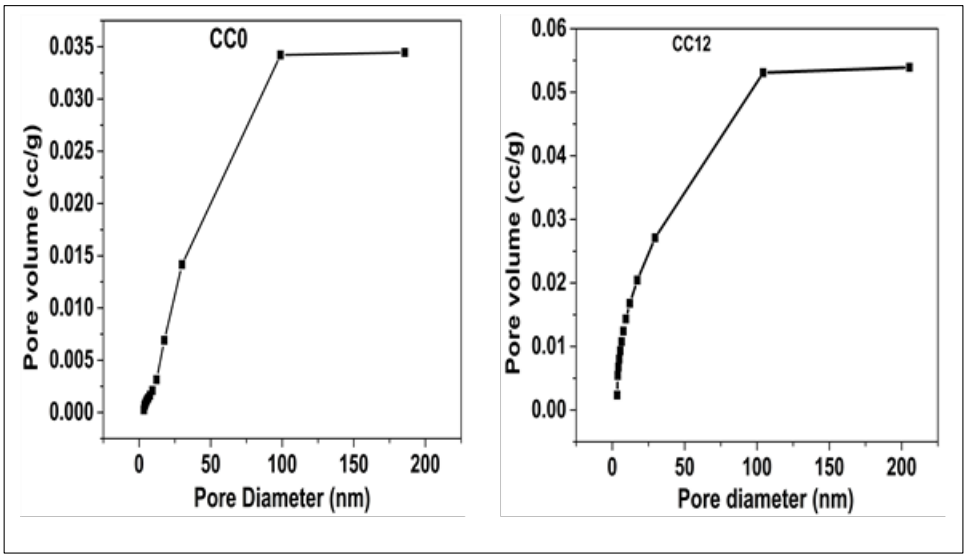

Fig. 7. Barrett-Joyner-Halenda (BJH) pore size distribution plot of CC0 and CC12.

pore size distribution of synthesized materials were measured using the BJH (Fig. 7) and BET nitrogen adsorption/desorption techniques. According to the IUPAC classification, the isotherms (Fig. 6) show type IV pore structures, which are typical of mesoporous materials. Sample CC0 and CC12 have been studied through BET and found that the surface area of the CC12 has been increased due to the addition of surfactant.

Raman spectra

The Raman spectra of CC0, CC4, CC8, and CC12 have been shown in Fig. 8(a). From closed observation of the obtained spectra, we found a wide peak in the range of 200 cm^{-1} to 500 cm^{-1} and a feeble band at around 940 cm^{-1}. Because of the asymmetric feature of this broad peak, one can easily notice that it is made up of more than one Raman band. So Lorentzian function is used for fitting the broad peak to find out the Raman Bands as shown in Fig. 8(b) and by this Lorentzian fitting we found the best fit at 267cm^{-1}, 311cm^{-1}, and 387cm^{-1} [**45**]–[**47**]. The position of the bands and

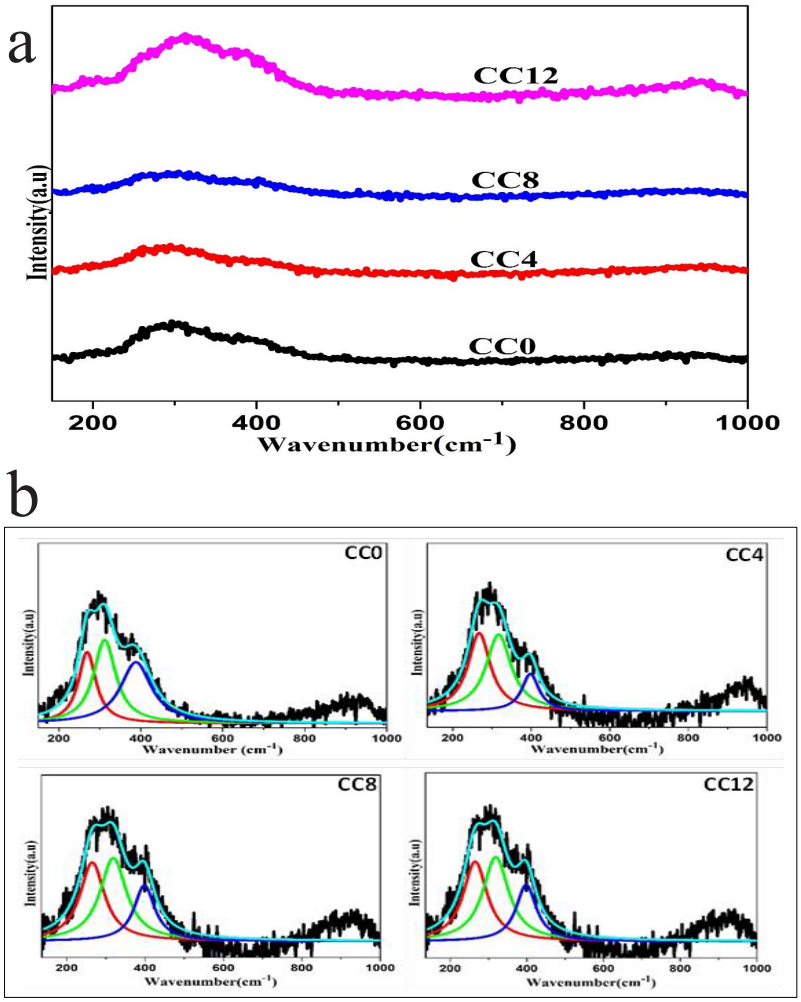

Fig. 8(a). Raman spectral image of prepared samples. 8(b). Fitted Raman spectra of prepared samples.

the shift in their positions are shown in Table 3.

The band centered at 267 cm^{-1} is allocated for 2TA(L) mode and the peaks at 310 cm^{-1} and 387 cm^{-1} are allotted for 2LA overtones of the Brillouin zone. The band nearly at 940 cm^{-1} is allocated for 2LO mode. Changes in the modes of vibration due to the addition of surfactant are compiled in Table 3. The band at 267 cm^{-1} is relocated by 4 cm^{-1} towards blue. The band at 311 cm^{-1} is relocated by 10 cm^{-1} towards blue. But the band at 388 cm^{-1} shifted blue up to CC8, but again it came to the same value. The presence of these peaks confirms the longitudinal optical (LO) as well as Transverse Optical (TO) modes in cubic CdO structures. The Nanoscale of CdO particles are responsible for these type of modes [**48**], [**49**]. These types of modes arise due to the second-order Raman scattering [**47**]. Due to the larger size of the crystallite, the CC12 peak intensity is also increased. The shifting of peaks is due to phonon confinement [**50**].

FTIR analysis

FTIR is a very useful optical technique to find out which types of functional groups are present in the material. The spectra of FTIR of all the prepared particles are revealed in Fig. 9. In FTIR spectra, bands are present at ~1740cm^{-1}, ~1370 cm^{-1}, ~1220 cm^{-1}, ~855 cm^{-1}, ~710 cm^{-1} and ~530 cm^{-1}. The band at ~1740 cm^{-1} represents the stretching of C=O [**51**], [**52**]. The band at around 1370 cm^{-1} is attributed to C-H stretching vibrations. The bands appearing at ~1220 cm^{-1} and ~855cm^{-1} are allotted to the vibrational bands of CO_3^{2-} CO_3^{2-} [**53**]. Small amounts of CO_2 are dissolved in water as a result of its presence in the atmosphere. In

Table 2. Parameters calculated from BET analyses.

CC0	CC4	CC8	CC12	Mode of Vibrations	Reference
269	267	265	273	2TA(L)	265
311	317	318	321	2LA	300
388	397	398	388	2LA	390
933	943	941	930	2LO	940

Table 3. After fitting of Raman spectra, the position of peaks (cm^{-1}) in Raman spectra.

Photocatalyst	Dye	Light Source	Degradation efficiency (%)	Degradation time (minutes)	References
CdO	MB	UV	65	110	[44]
CdO	MB	Sunlight	78	90	[48]
CdO	MB	UV	80	120	[54]
CdO	MB	UV	83	80	Present work

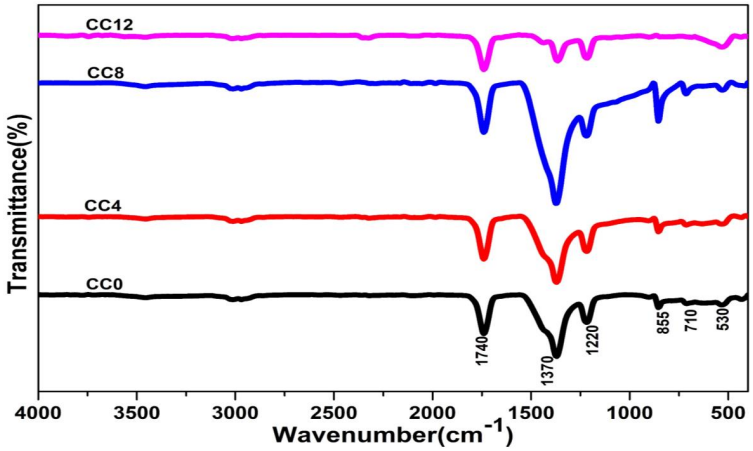

Fig. 9 FTIR spectra of prepared samples for identification of chemical composition.

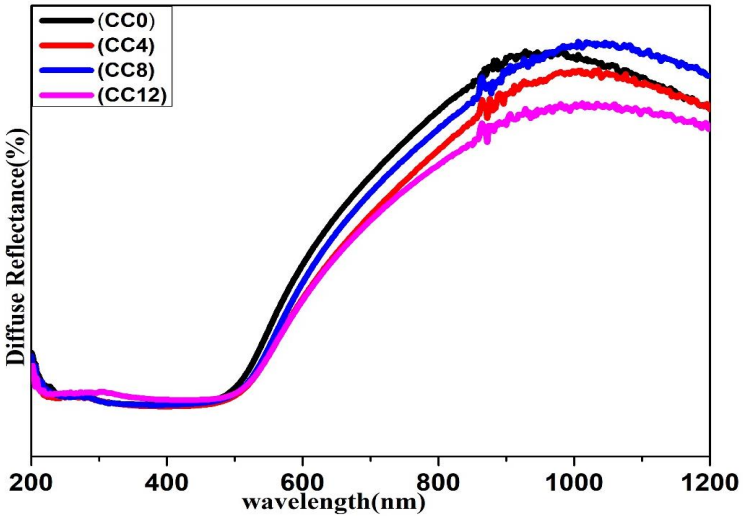

Fig. 10. Diffused Reflectance Spectra of prepared samples.

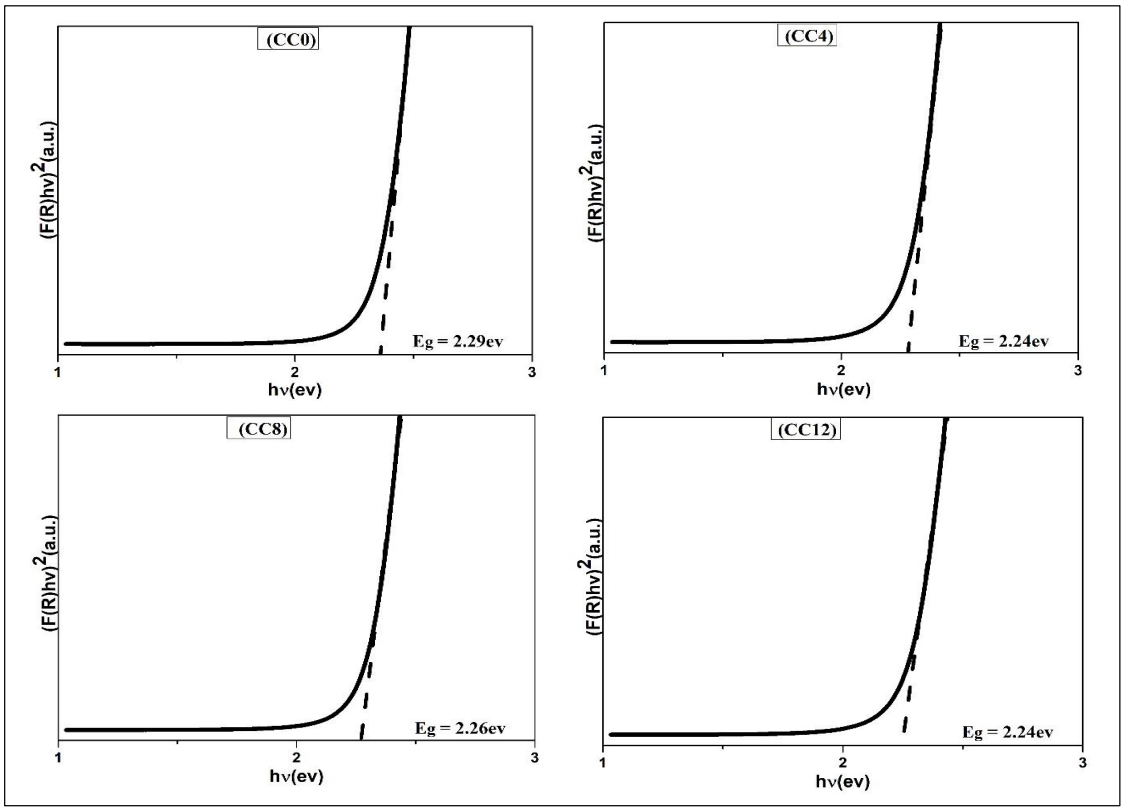

Fig. 11. Kubelka-Munk plot for calculation of direct band gap for (a) CC0 (b) CC4 (c) CC8 (d) CC12.

an equilibrium, carbon dioxide and carbonic acid coexist in aqueous solution. Because this acid is so weak, only trace amounts of carbonate are formed by this chemical equilibrium. Generally, bands less than 1000 cm^{-1} help to find out the metal oxide bonds [**54**]. The weak band at ~710 cm^{-1} corresponds to the Cd-O phase [**51**]. 531 cm^{-1} band is the stretching mode of vibration of CdO The majority of metal compounds should be found in this region [**55**], [**56**].

Diffused Reflectance Spectroscopy

Surfactant limits the growth of particles by adsorption on the surface. Variations in the concentration of surfactant will affect the growth of particles in a different manner. Along with the particle size of CdO, the effects of surfactant concentration on the optical properties have been studied through Diffused Reflectance Spectra (DRS). Diffused Reflectance Spectra of synthesized samples have been shown in Fig. 10. It illustrates that the concentration of surfactant does not affect the reflectance edge of spectra and also reveals that the characteristic absorption edge is near 500 nm for all samples. Equation (5) is the Kubelka-Munk function [**9**], [**57**]–[**60**] which is used to find out the optical band gap of material from Diffused Reflectance Spectra.

$$F(R) = \frac{(1-R)^2}{2R} \quad (5)$$

Here R represents reflectance in percentage. A Graph between $(F(R)hv)^n$ and hv has been plotted. Value of n=2 is reserved for the direct allowed band gap and n=1/2 is reserved for the indirect allowed band gap. h and v stand for their usual meaning Planck's constant and frequency respectively. Extending the straight segment of the plot to intersect at the x-axis finds the optical band gap (Eg) of the prepared samples (as revealed in Fig. 11). The values of the intersection at the x-axis of the optical band gap are compiled in Table 1. From Fig. 11 we can see that as we increased the concentration of CTAB surfactant, the band gap of the material decreased by 0. 05 eV. Increasing concentration of CTAB leads to an increase in

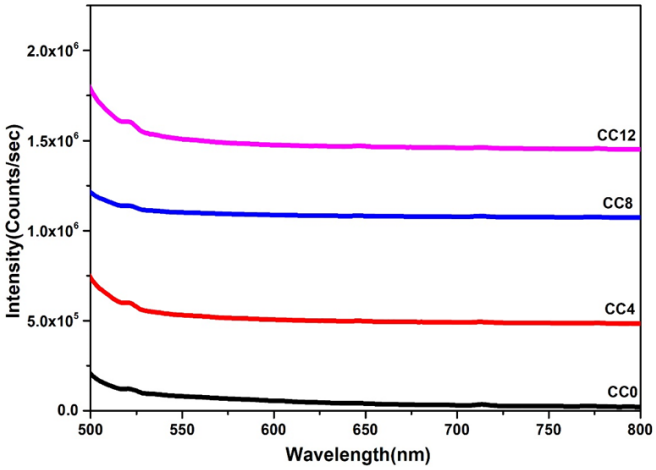

Fig. 12. PL emission spectra of samples excited at 470 nm.

structural disorder and defects. The band gap has decreased which may be due to the preparation condition and creation of allowed energy states in the band gap of the CdO nanoparticles. The values of the optical band gap of the CC0 and CC12 are 2.29 eV and 2.24 eV respectively.

Photoluminescence Spectra

470 nm was used as the excitation wavelength for measuring the photoluminescence spectra of the prepared samples. The Spectra of the material are shown in Fig. 12. Spectra is found to comprise a peak positioned at ~521 nm which is the emission peak of recombination of holes produced from photon and oxygen vacancy **[61]**. 521 nm lies in the range of green emission which is due to interstitial vacancies and oxygen vacancies **[62]**. From the spectra, it has been found that the addition of surfactant does not affect the intensity of the peak because it is not creating any kind of defects in the crystal. Surfactant rather aligns the particles in a particular direction instead of creating defects or oxygen vacancies in the CdO.

PHOTOCATALYTIC ACTIVITY

The photocatalytic ability of the cadmium oxide nanoparticles is assessed by the deterioration of dye (MB) with the help of a UV light source. The absorbance range of MB dye is from wavelength 500 to 700 nm. From the literature survey, a comparison of the photocatalytic performance of cadmium oxide has been done and is given in Table 4.

Fig. 13 (a-d) shows the absorbance spectra of MB dye with time when treated with CC0, CC4, CC8, and CC12 respectively. After analyzing the absorption spectra of MB dye in the presence of various prepared CTAB-assisted CdO nanoparticles, as time progresses, the intensity of MB dye's major absorption peak is becoming less and less intense at 664 nm. Using the absorption spectra, the % breakdown of MB dye has been evaluated using equation 1 (given in the experimental section). % Degradation is found in the order of 83% with CC0, 82% with CC4, 70% with CC8, and 74% with CC12 as shown in Fig. 14. As maximum degradation is obtained in the case of pure CdO, degradation of Rose Bengal (RB) dye has been studied in presence of CdO using visible light. The absorption spectra of RB are shown in Fig. 15. From spectra, it is found that the Rose Bengal dye degrades up to 85% within 80 minutes of light illumination.

The main contribution to the degradation of dye by a photocatalyst is photons. As we know when we irradiate the sample with radiation having energy equivalent or higher from the band gap of the material electron from the valence band jump to the conduction band leaving behind a hole in the valence band. These e^- and h^+ react with atmospheric oxygen and water molecules leading to the formation of oxidant super oxygen anionic radical ($^{\bullet}O_2^-$) and hydroxyl radicals ($^{\bullet}OH$) respectively as shown in Fig. 1. These oxidant species react with harmful dyes and convert them into non-harmful by-products. The band gap and absorbency of the nanoparticles affect the photocatalytic activity. When a photocatalyst shows higher absorbency towards photons, the

Table 4. Comparative results of photocatalytic performance of cadmium oxide nanoparticles through literature survey.

Photocatalyst	Dye	Light Source	Degradation efficiency (%)	Degradation time (minutes)	References
CdO	MB	UV	65	110	[49]
CdO	MB	Sunlight	78	90	[53]
CdO	MB	UV	80	120	[59]
CdO	MB	UV	83	80	Present work

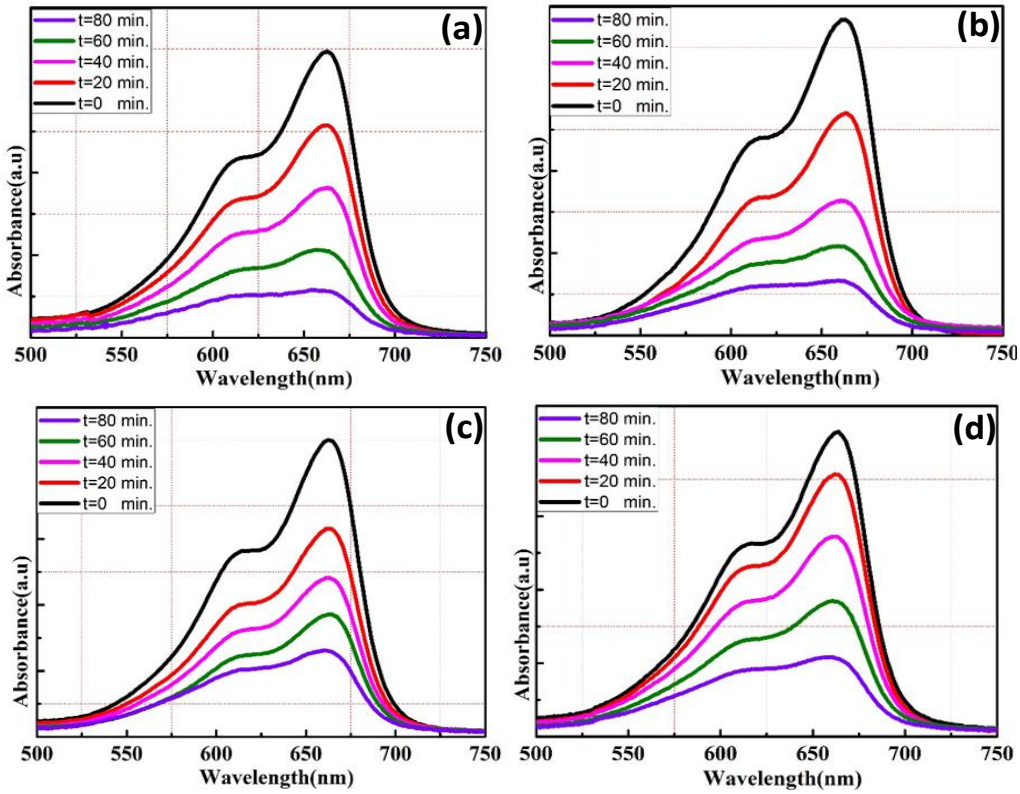

Fig. 13. Degradation of MB dye in the presence of UV light with (a) CC0 (b) CC4 (c) CC8 (d) CC12.

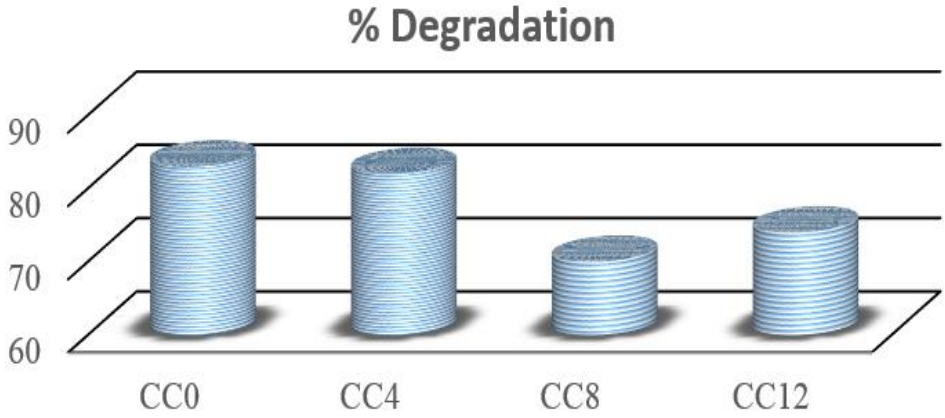

Fig. 14. Degradation (%) graphs of MB dye by the samples.

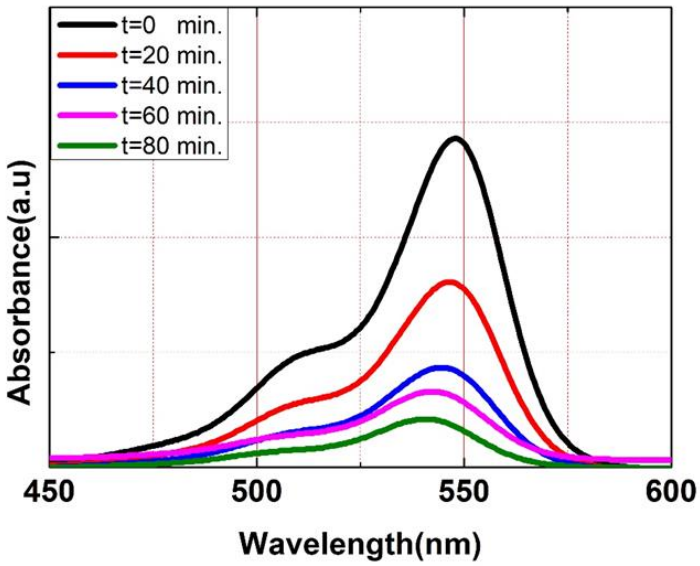

Fig. 15. Degradation of RB dye in sunlight with CC0.

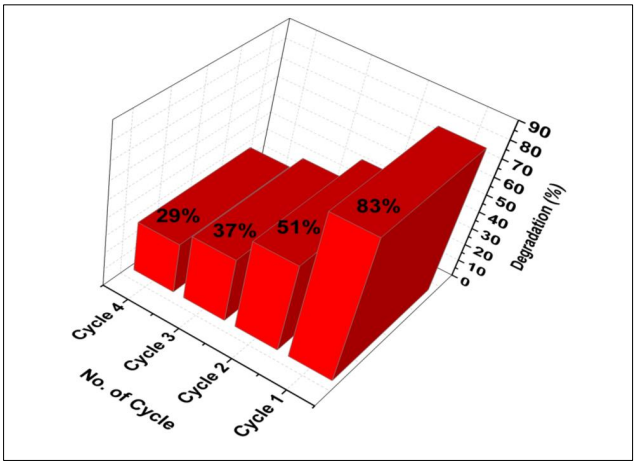

Fig. 16. The experiment of catalytic cycles of CC0.

creation of more electrons and holes takes place. Due to more numbers of electron and hole pairs photocatalytic efficiency also increases. But again, the combination of electrons and holes can decrease the efficiency of the nanoparticles. The surface area plays a vital role in the photocatalytic process. More area on the surface means the presence of active sites in greater numbers on the surface. These active sites act as trap centers for electrons and holes to avoid their recombination [**28**]. The presence of dangling bonds on the planes helps in the adsorption of hydroxyl ions [·OH] due to the positive charge of the planes and the production of hydroxyl free radicals [·OH] takes place [**63**]. These free radicals enhance the photocatalytic performance of the nanoparticles. But in this work, due to the addition of surfactant photocatalytic activity is decreasing because the surface area is changing from nanosheets to needle-like structure. These needle-like structures are very dense so these surface-active sites are unable to take part in photocatalytic reactions. So pure CdO is showing higher photocatalytic activity. The experiment of catalytic cycles (Fig.16) of CC0 was performed up to four cycles, and it was discovered that the sample can be used as an efficient photocatalyst for up to 2 cycles.

CONCLUSION

Pure CdO nanoparticles synthesized with a feasible co-precipitation method performed highly efficiently in comparison to CTAB-assisted CdO nanoparticles in the degradation of MB dye in 80 minutes. XRD confirmed the formation of the well-crystalline nature of prepared samples. Variation in surfactant concentration modified the morphology of flat-sheet into thin needle-like structures confirmed by FESEM. The presence of functional groups is confirmed by FTIR. The effect of the addition of surfactant on phonon confinement can be seen in Raman spectra. Degradation efficiency decreased from 83% to 74% because the flat sheet has more trap centers to capture electrons in comparison to the thin needle. Hydrophobic interactions between surfactant molecules play a vital role in aligning the particle in a particular direction. Therefore, this study indicates that surfactants can be used as potential material to change the morphology of the particles. The prepared CdO nanoparticles are found to be a promising photocatalyst in the degradation of MB and RB dye with degradation up to 83% and 85% respectively.

DECLARATION

ACKNOWLEDGMENT

Among the authors, in connection with the present project, Deepak (JRF Award letter No. 09/1063(0024)/2019) wishes to express his appreciation and gratitude to CSIR for the financial assistance.

CONFLICT OF INTEREST

No conflict of interest exists among the authors.

REFERENCES

[1] Shokri, A. (2019). Application of electrocoagulation process for the removal of Acid orange 5 in synthetic wastewater. Iranian Journal of Chemistry and Chemical Engineering (IJCCE), 38(2), 113-119. https://doi.org/10.30492/ijcce.2019.30593

[2] M. Saghi, A. Shokri, A. Arastehnodeh, M. Khazaeinejad, and A. Nozari, "The photo degradation of methyl red in aqueous solutions by α-Fe2O3/SiO2 nano photocatalyst," J. Nanoanalysis, vol. 5, no. 3, pp. 163-170, 2018, doi: 10.22034/jna.2018.542765.

[3] Shokri, A. (2018). Employing electro coagulation for the removal of Acid Red 182 in aqueous environment using Box-Behenken design method. Desalination and Water Treatment, 115, 281-287. http://dx.doi.org/10.5004/dwt.2018.22451

[4] Shokri, A., Salimi, M. and Abmatin, T., 2017. Employing photo Fenton and UV/ZnO processes for removing Reactive red 195 from aqueous environment. Fresenius Environmental Bulletin, 26(2-A), pp.1560-1565.

[5] Shokri, A. and Karimi, S., 2020. Treatment of aqueous solution containing acid red 14 using an electro peroxone process and a box-Behnken experimental design. Archives of Hygiene Sciences, 9(1), pp.48-57. http://dx.doi.org/10.29252/ArchHygSci.9.1.48

[6] A. Khatri and P. S. Rana, "Visible light photocatalysis of methylene blue using cobalt substituted cubic NiO nanoparticles," Bull. Mater. Sci., vol. 42, no. 4, Aug. 2019, https://doi.org/10.1007/s12034-019-1835-z

[7] A. Khatri and P. S. Rana, "Visible light assisted photocatalysis of Methylene Blue and Rose Bengal dyes by iron doped NiO nanoparticles prepared via chemical co-precipitation," Phys. B Condens. Matter, vol. 579, Feb. 2020, https://doi.org/10.1016/j.physb.2019.411905

[8] A. Khatri and P. S. Rana, "Visible Light Assisted Enhanced Photocatalytic Performance of ZnO/NiO Nanocomposites Prepared by Chemical Co-Precipitation Method," J. Nanosci. Nanotechnol., vol. 19, no. 8, pp. 5233-5240, Mar. 2019, https://doi.org/10.1166/jnn.2019.16835

[9] G. Crini and E. Lichtfouse, "Advantages and disadvantages of techniques used for wastewater treatment," Environ. Chem. Lett., vol. 17, no. 1, pp. 145-155, 2019, https://doi.org/10.1007/s10311-018-0785-9

[10] K. G. Pavithra, S. K. P., V. Jaikumar, and S. R. P., "Removal of colorants from wastewater: A review on sources and treatment strategies," J. Ind. Eng. Chem., vol. 75, pp. 1-19, 2019, https://doi.org/10.1016/j.jiec.2019.02.011

[11] S. Balachandran, S. G. Praveen, R. Velmurugan, and M. Swaminathan, "Facile fabrication of highly efficient, reusable heterostructured Ag-ZnO-CdO and its twin applications of dye degradation under natural sunlight and self-cleaning," RSC Adv., vol. 4, no. 9, pp. 4353-4362, 2014, https://doi.org/10.1039/C3RA45381B

[12] S. Sarkar, N. T. Ponce, A. Banerjee, R. Bandopadhyay, S. Rajendran, and E. Lichtfouse, "Green polymeric nanomaterials for the photocatalytic degradation of dyes: a review," Environ. Chem. Lett., vol. 18, no. 5, pp. 1569-1580, 2020, https://doi.org/10.1007/s10311-020-01021-w

[13] K. Hashimoto, H. Irie, and A. Fujishima, "TiO 2 photocatalysis: A historical overview and future prospects," Japanese J. Appl. Physics, Part 1 Regul. Pap. Short Notes Rev. Pap., vol. 44, no. 12, pp. 8269-8285, 2005, https://doi.org/10.1143/JJAP.44.8269

[14] A. Salem, "Silver-doped cadmium oxide nanoparticles: Synthesis, structural and optical properties," Eur. Phys. J. Plus, vol. 129, no. 12, 2014, https://doi.org/10.1140/epjp/i2014-14263-3

[15] A. Harriman, "Photoelectrochemical studies with n-type Cdo," J. Chem. Soc. Faraday Trans. 1 Phys. Chem. Condens. Phases, vol. 79, no. 12, pp. 2875-2877, 1983, https://doi.org/10.1039/f19837902875

[16] N. Wongcharoen, T. Gaewdang, and T. Wongcharoen, "Electrical properties of Al-doped CdO thin films prepared by thermal evaporation in vacuum," Energy Procedia, vol. 15, no. 2011, pp. 361-370, 2012, https://doi.org/10.1016/j.egypro.2012.02.044

[17] M. R. Alam, M. Mozibur Rahman, A. M. M. Tanveer Karim, and M. K. R. Khan, "Effect of Ag incorporation on structural and opto-electric properties of pyrolized CdO thin films," Int. Nano Lett., vol. 8, no. 4, pp. 287-295, 2018, https://doi.org/10.1007/s40089-018-0251-5

[18] M. Çavaş, F. Yakuphanoğlu, and Karataş, "The electrical

properties of photodiodes based on nanostructure gallium doped cadmium oxide/p-type silicon junctions," Indian J. Phys., vol. 91, no. 4, pp. 413-420, 2017, https://doi.org/10.1007/s12648-016-0952-4

[19] K. Usharani, A. R. Balu, V. S. Nagarethinam, and M. Suganya, "Characteristic analysis on the physical properties of nanostructured Mg-doped CdO thin films-Doping concentration effect," Prog. Nat. Sci. Mater. Int., vol. 25, no. 3, pp. 251-257, 2015, https://doi.org/10.1016/j.pnsc.2015.06.003

[20] Z. Zhao, D. L. Morel, and C. S. Ferekides, "Electrical and optical properties of tin-doped CdO films deposited by atmospheric metalorganic chemical vapor deposition," Thin Solid Films, vol. 413, no. 1-2, pp. 203-211, 2002, https://doi.org/10.1016/S0040-6090(02)00344-9

[21] A. A. Dakhel, "Influence of hydrogenation on the electrical and optical properties of CdO thin films," Semicond. Sci. Technol., vol. 23, no. 5, 2008, https://doi.org/10.1088/0268-1242/23/5/055017

[22] A. A. Dakhel, "Development of electrical conduction with beryllium doping of CdO nanostructure thin Films," Mater. Res., vol. 18, no. 1, pp. 222-227, 2015, https://doi.org/10.1590/1516-1439.301014

[23] R. Aydin, B. Sahin, and F. Bayansal, "Sodium dodecyl sulfate-assisted SILAR synthesis of nanostructured cadmium oxide films," Ceram. Int., vol. 42, no. 10, pp. 11822-11826, 2016, https://doi.org/10.1016/j.ceramint.2016.04.103

[24] B. Arif et al., "Optical properties of Zn1−xAlxO:NiO transparent metal oxide composite thin films prepared by sol-gel method," J. Sol-Gel Sci. Technol., vol. 76, no. 2, pp. 378-385, 2015, https://doi.org/10.1007/s10971-015-3786-1

[25] S. U. Park and J. H. Koh, "Low temperature rf-sputtered in and Al co-doped ZnO thin films deposited on flexible PET substrate," Ceram. Int., vol. 40, no. 7 PART A, pp. 10021-10025, 2014, https://doi.org/10.1016/j.ceramint.2014.02.101

[26] N. Al Dahoudi, "Comparative study of highly dense aluminium- and gallium-doped zinc oxide transparent conducting sol-gel thin films," Bull. Mater. Sci., vol. 37, no. 6, pp. 1243-1248, 2014, https://doi.org/10.1007/s12034-014-0068-4

[27] B. Hymavathi, B. R. Kumar, and T. S. Rao, "Structural, Surface Morphological and Optical Properties of Cr Doped CdO Thin Films for Optoelectronic Devices," Mater. Today Proc., vol. 2, no. 4-5, pp. 1510-1517, 2015, https://doi.org/10.1016/j.matpr.2015.07.077

[28] K. Karthik, S. Dhanuskodi, C. Gobinath, S. Prabukumar, and S. Sivaramakrishnan, "Photocatalytic and antibacterial activities of hydrothermally prepared CdO nanoparticles," J. Mater. Sci. Mater. Electron., vol. 28, no. 15, pp. 11420-11429, 2017, https://doi.org/10.1007/s10854-017-6937-z

[29] R. K. Gupta, K. Ghosh, R. Patel, S. R. Mishra, and P. K. Kahol, "Structural, optical and electrical properties of In doped CdO thin films for optoelectronic applications," Mater. Lett., vol. 62, no. 19, pp. 3373-3375, 2008, https://doi.org/10.1016/j.matlet.2008.03.015

[30] M. Ravikumar, S. Valanarasu, R. Chandramohan, S. S. K. Jacob, and A. Kathalingam, "Effect of Trisodium Citrate Concentration on the Structural and Photodiode Performance of CdO Thin Films," J. Electron. Mater., vol. 44, no. 8, pp. 2800-2806, 2015, https://doi.org/10.1007/s11664-015-3759-8

[31] M. Zaien, N. M. Ahmed, and Z. Hassan, "Fabrication and characterization of nanocrystalline n-CdO/p-Si as a solar cell," Superlattices Microstruct., vol. 52, no. 4, pp. 800-806, 2012, https://doi.org/10.1016/j.spmi.2012.06.028

[32] T. Singh, D. K. Pandya, and R. Singh, "Annealing studies on the structural and optical properties of electrodeposited CdO thin films," Mater. Chem. Phys., vol. 130, no. 3, pp. 1366-1371, 2011, https://doi.org/10.1016/j.matchemphys.2011.09.035

[33] R. Chandiramouli and B. G. Jeyaprakash, "Review of CdO thin films," Solid State Sci., vol. 16, pp. 102-110, 2013, https://doi.org/10.1016/j.solidstatesciences.2012.10.017

[34] M. Parashar, V. K. Shukla, and R. Singh, "Metal oxides nanoparticles via sol-gel method: a review on synthesis, characterization and applications," J. Mater. Sci. Mater. Electron., vol. 31, no. 5, pp. 3729-3749, 2020, https://doi.org/10.1007/s10854-020-02994-8

[35] H. Hayashi and Y. Hakuta, "Hydrothermal Synthesis of metal oxide nanoparticles in supercritical water," Materials (Basel)., vol. 3, no. 7, pp. 3794-3817, 2010, https://doi.org/10.3390/ma3073794

[36] M. Mukhtar, L. Munisa, and R. Saleh, "Co-Precipitation Synthesis and Characterization of Nanocrystalline Zinc Oxide Particles Doped with Cu²⁺ Ions," Mater. Sci. Appl., vol. 03, no. 08, pp. 543-551, 2012, https://doi.org/10.4236/msa.2012.38077

[37] A. Rajaeiyan and M. M. Bagheri-Mohagheghi, "Comparison of sol-gel and co-precipitation methods on the structural properties and phase transformation of γ and α-Al2O3 nanoparticles," Adv. Manuf., vol. 1, no. 2, pp. 176-182, 2013, https://doi.org/10.1007/s40436-013-0018-1

[38] M. C. Mascolo, Y. Pei, and T. A. Ring, "Room Temperature Co-Precipitation Synthesis of Magnetite Nanoparticles in a Large ph Window with Different Bases," Materials (Basel)., vol. 6, no. 12, pp. 5549-5567, 2013, https://doi.org/10.3390/ma6125549

[39] B. Sahin, F. Bayansal, M. Yuksel, N. Biyikli, and H. A. Çetinkara, "Effect of coumarin concentration on the physical properties of CdO nanostructures," Ceram. Int., vol. 40, no. 4, pp. 5237-5243, 2014, https://doi.org/10.1016/j.ceramint.2013.10.093

[40] M. Moradi, E. Solati, S. Darvishi, and D. Dorranian, "Effect of Aqueous Ablation Environment on the Characteristics of ZnO Nanoparticles Produced by Laser Ablation," J. Clust. Sci., vol. 27, no. 1, pp. 127-138, 2016, https://doi.org/10.1007/s10876-015-0915-5

[41] A. K. Ramasami, M. V. Reddy, and G. R. Balakrishna, "Combustion synthesis and characterization of NiO nanoparticles," Mater. Sci. Semicond. Process., vol. 40, pp. 194-202, 2015, https://doi.org/10.1016/j.mssp.2015.06.017

[42] S. Kumar, B. Ahmed, A. K. Ojha, J. Das, and A. Kumar, "Facile synthesis of CdO nanorods and exploiting its properties towards supercapacitor electrode materials and low power UV irradiation driven photocatalysis against methylene blue dye," Mater. Res. Bull., vol. 90, pp. 224-231, 2017, https://doi.org/10.1016/j.materresbull.2017.02.044

[43] S. Anjum, S. Shaheen, M. S. Awan, and R. Zia, "Effect of various surfactants on optical and electrical properties of Cu+2-doped ZnS semiconductor nanoparticles," Appl. Phys. A Mater. Sci. Process., vol. 125, no. 4, pp. 1-10, 2019, https://doi.org/10.1007/s00339-019-2558-0

[44] I. K. Punithavathi, M. Elayaraja, S. J. Jeyakumar, and M. Jothibas, "Synthesis and characterization of surfactants (CTAB and PEG) assisted CdO nanoparticles," vol. 9, no. 7, pp. 37-46.

[45] S. Kumar and A. K. Ojha, "Synthesis, characterizations and antimicrobial activities of well dispersed ultra-long CdO nanowires," AIP Adv., vol. 3, no. 5, 2013, https://doi.org/10.1063/1.4804930

[46] S. Kumar, A. K. Ojha, and R. K. Singh, "Synthesis and Raman signature for the formation of CdO/MnO2 (core/shell) nanostructures," J. Raman Spectrosc., vol. 45, no. 9, pp. 717-722, 2014, https://doi.org/10.1002/jrs.4537

[47] R. Cuscó, J. Ibáñez, N. Domenech-Amador, L. Artús, J. Zúiga-•rez, and V. Muoz-Sanjoś, "Raman scattering of cadmium oxide epilayers grown by metal-organic vapor phase epitaxy," J. Appl. Phys., vol. 107, no. 6, 2010, https://doi.org/10.1063/1.3357377

[48] F. T. Thema, P. Beukes, A. Gurib-Fakim, and M. Maaza, "Green synthesis of Monteponite CdO nanoparticles by Agathosma betulina natural extract," J. Alloys Compd., vol. 646, pp. 1043-1048, 2015, https://doi.org/10.1016/j.jallcom.2015.05.279

[49] S. Kumar, A. K. Ojha, and B. Walkenfort, "Cadmium oxide nanoparticles grown in situ on reduced graphene oxide for enhanced photocatalytic degradation of methylene blue dye under ultraviolet irradiation," J. Photochem. Photobiol. B Biol., vol. 159, pp. 111-119, 2016, https://doi.org/10.1016/j.jphotobiol.2016.03.025

[50] I. Iatsunskyi, S. Jurga, V. Smyntyna, M. Pavlenko, V. Myndrul, and A. Zaleska, "Raman spectroscopy of nanostructured silicon fabricated by metal-assisted chemical etching," Opt. Micro- Nanometrology V, vol. 9132, p. 913217, 2014, https://doi.org/10.1117/12.2051489

[51] A. T. Ravichandran, A. Robert Xavier, K. Pushpanathan, B. M. Nagabhushana, and R. Chandramohan, "Structural and optical properties of Zn doped CdO nanoparticles synthesized by chemical precipitation method," J. Mater. Sci. Mater. Electron., vol. 27, no. 3, pp. 2693-2700, 2016, https://doi.org/10.1007/s10854-015-4079-8

[52] R. Nallendran, G. Selvan, and A. R. Balu, "Photocatalytic Performance of SnO 2 Coupled CdO Nanoparticles Against MY and RhB Dyes," J. Electron. Mater., vol. 48, no. 6, pp. 3676-3685, 2019, https://doi.org/10.1007/s11664-019-07125-6

[53] A. Taufik, H. Tju, S. P. Prakoso, and R. Saleh, "Different routes of synthesized CdO nanoparticles through microwave-assisted methods and photocatalytic study," AIP Conf. Proc., vol. 2023, no. 2018, pp. 10-15, 2018, https://doi.org/10.1063/1.5064032

[54] K. Gurumurugan, D. Mangalaraj, and S. K. Narayandass, "Magnetron sputtered transparent conducting CdO thin films," J. Electron. Mater., vol. 25, no. 5, pp. 765-770, 1996, https://doi.org/10.1007/BF02666538

[55] T. Athar, S. S. M. Shafi, and A. A. Khan, "Soft Chemical Process for Synthesis of CdO Nanoparticles," Mater. Focus, vol. 3, no. 5, pp. 397-400, 2014, https://doi.org/10.1166/mat.2014.1194

[56] R. Ranjithkumar, A. Albert Irudayaraj, G. Jayakumar, A. Dhayal Raj, S. Karthick, and R. Vinayagamoorthy, "Synthesis and Properties of CdO and Fe doped CdO Nanoparticles," Mater. Today Proc., vol. 3, no. 6, pp. 1378-1382, 2016, https://doi.org/10.1016/j.matpr.2016.04.018

[57] P. Kubelka, "New Contributions to the Optics of Intensely Light-Scattering Materials Part II: Nonhomogeneous Layers*," J. Opt. Soc. Am., vol. 44, no. 4, p. 330, 1954, https://doi.org/10.1364/JOSA.44.000330

[58] L. Yang and B. Kruse, "Revised Kubelka-Munk theory I Theory and application," J. Opt. Soc. Am. A, vol. 21, no. 10, p. 1933, 2004, https://doi.org/10.1364/JOSAA.21.001933

[59] G. Somasundaram, J. Rajan, P. Sangaiya, and R. Dilip, "Hydrothermal synthesis of CdO nanoparticles for photocatalytic and antimicrobial activities," Results Mater., vol. 4, p. 100044, 2019, https://doi.org/10.1016/j.rinma.2019.100044

[60] L. Yang and S. J. Miklavcic, "Revised Kubelka-Munk theory III A general theory of light propagation in scattering and absorptive media," J. Opt. Soc. Am. A, vol. 22, no. 9, p. 1866, 2005, https://doi.org/10.1364/JOSAA.22.001866

[61] D. B. Bharti and A. V. Bharati, "Photocatalytic degradation of Alizarin Red dye under visible light using ZnO & CdO nanomaterial," Optik (Stuttg)., vol. 160, pp. 371-379, 2018, https://doi.org/10.1016/j.ijleo.2018.01.122

[62] B. Goswami and A. Choudhury, "Enhanced visible luminescence and modification in morphological properties of cadmium oxide nanoparticles induced by annealing," J. Exp. Nanosci., vol. 10, no. 12, pp. 900-910, 2015, https://doi.org/10.1080/17458080.2014.933492

[63] M. P. Rao, S. Anandan, S. Suresh, A. M. Asiri, and J. J. Wu, "Surfactant Assisted Synthesis of Copper Oxide Nanoparticles for Photocatalytic Degradation of Methylene Blue in the Presence of Visible Light," Energy Environ. Focus, vol. 4, no. 3, pp. 250-255, 2015, https://doi.org/10.1166/eef.2015.1168